Title

Heparan Sulfate Glycosaminoglycans in Glioblastoma Promote Tumor Invasion

Journal

Molecular Cancer Research, 15(11)

ISSN

1541-7786

Authors

Tran, Vy M

Wade, Anna

McKinney, Andrew

et al.

Publication Date

2017-11-01

DOI

10.1158/1541-7786.mcr-17-0352

Peer reviewed

HHS Public Access

Author manuscript

Mol Cancer Res. Author manuscript; available in PMC 2018 July 25.

Published in final edited form as:

Mol Cancer Res. 2017 November ; 15(11): 1623–1633. doi:10.1158/1541-7786.MCR-17-0352.

Heparan Sulfate Glycosaminoglycans in Glioblastoma Promote Tumor Invasion

Vy M Tran[1], **Anna Wade**[1], **Andrew McKinney**[1], **Katharine Chen**[1], **Olle R. Lindberg**[1], **Jane R. Engler**[1], **Anders I. Persson**[1,2,3], and **Joanna J. Phillips**[1,2,3,4,*]

[1]Department of Neurological Surgery, Brain Tumor Center, University of California, San Francisco, San Francisco, CA, USA. 94158

[2]Helen Diller Family Comprehensive Cancer Center, University of California, San Francisco, San Francisco, CA 94158

[3]Sandler Neurosciences Center, Department of Neurology, University of California, San Francisco, CA, 94158

[4]Department of Pathology, Division of Neuropathology, University of California, San Francisco, San Francisco, CA 94143

Abstract

Glioblastoma (GBM) is the most common primary malignant brain tumor of adults and confers a poor prognosis due, in part, to diffuse invasion of tumor cells. Heparan sulfate (HS) glycosaminoglycans, present on the cell surface and in the extracellular matrix, regulate cell signaling pathways and cell-microenvironment interactions. In GBM, the expression of HS glycosaminoglycans and the enzymes that regulate their function are altered but the actual HS content and structure are unknown. However, inhibition of HS glycosaminoglycan function is emerging as a promising therapeutic strategy for some cancers. In this study, we use liquid chromatography-mass spectrometry (LC/MS) analysis to demonstrate differences in HS disaccharide content and structure across four patient-derived tumorsphere lines (GBM1, 5, 6, 43) and between two murine tumorsphere lines derived from murine GBM with enrichment of mesenchymal and proneural gene expression (mMES and mPN, respectively) markers. In GBM, the heterogeneous HS content and structure across patient-derived tumorsphere lines suggested diverse functions in the GBM tumor microenvironment (TME). In GBM5 and mPN, elevated expression of sulfatase 2 (SULF2), an extracellular enzyme that alters ligand binding to HS, was associated with low trisulfated HS disaccharides, a substrate of SULF2. In contrast, other primary tumorsphere lines had elevated expression of the HS-modifying enzyme heparanase (HPSE). Using gene editing strategies to inhibit HPSE a role for HPSE in promoting tumor cell adhesion and invasion was identified. These studies characterize the heterogeneity in HS glycosaminoglycan content and structure across GBM and reveal their role in tumor cell invasion.

*Corresponding author: Joanna.phillips@ucsf.edu, The Helen Diller Family Cancer Research Building, 1450 Third Street, Room HD492B, Box 0520, University of California, San Francisco, San Francisco, CA 94143, Phone: 415-514-4929, FAX: 415-514-9792.

Conflicts of interest: The authors declare that they have no conflicts of interest with the contents of this article.

Keywords

Microenvironment; heparanase; invasion; GBM; SULFs

INTRODUCTION

Glioblastoma (GBM) is characterized by tumoral heterogeneity, including differences in tumor cell invasion and receptor tyrosine kinase (RTK) signaling pathway activity. Despite this heterogeneity transcriptional profiling has identified tumor subtypes (1,2) with enrichment of specific cell signaling (3), proteomic (4,5) and immune cell characteristics (6,7). The design of improved therapeutics for GBM requires an understanding of intertumoral heterogeneity and its potential impact on therapeutic response.

Heparan sulfate proteoglycans (HSPGs), present on the cell surface and in the extracellular matrix (ECM), are abundant in the brain and regulate interactions in the extracellular environment via their binding with diverse partners, including soluble factors, membrane proteins and the ECM (8). HSPGs consist of a core protein and covalently attached heparan sulfate (HS) glycosaminoglycan chains comprised of repeating disaccharide units. Extensive co- and post-translational enzymatic modifications, particularly involving the HS chains, generate the structural diversity important for their many functions, including their ability to bind and sequester soluble ligands, act as a co-receptor on the cell surface (9), and influence cell adhesion and migration, one mechanism being the regulation of integrin activity (8,10).

A major determinant of the specificity and the affinity of HSPG ligand interactions is the sulfation pattern of the HS glycosaminoglycan (GAG) side chains, for which one critical determinant is the 6-*O*-sulfate (6*OS*) of glucosamine (8,11). Regulation of 6OS levels occurs during biosynthesis and post-synthetically by the extracellular endoglucosamine-6-sulfatases or sulfatases (SULFs) whose principle substrate is trisulfated disaccharides (12). SULF1 or SULF2 desulfation of 6*OS* regulates HS-ligand binding and subsequent cell signaling important in normal development and in cancer, including Wnt, sonic hedgehog (Shh), fibroblast growth factor (FGF), vascular endothelial growth factor (VEGF), glial cell line-derived growth factor (GDNF), and stromal cell-derived factor 1 (SDF1) (13–17). In GBM, the expression of HSPGs and the enzymes that regulate their function, including SULF2, are altered (18). In human GBM cell lines and murine models for high grade glioma, SULF2 has been directly implicated in promoting tumorigenesis (19–21). Ablation of SULF2 in tumor-prone cells resulted in decreased tumor growth, prolonged host survival, increased HSPG 6-*O*-sulfation in tumors *in vivo*, and decreased activity of PDGFRα and related downstream signaling pathways (21).

Heparanase (HPSE), a β-endoglucuronidase, cleaves HS chains to reduce HS chain length and release smaller biologically active oligosaccharides. Increased HPSE activity is associated with increased tumorigenesis, angiogenesis and invasiveness in diverse cancers including multiple myeloma, melanoma, breast, and pancreatic cancer (22). In multiple myeloma, a number of oncogenic functions for HPSE have been identified including direct effects on tumor cells and indirect effects on tumor-associated endothelial cells (10,23,23–25). In the brain, HPSE has been implicated in metastatic tumor cell invasion and

medulloblastoma cell signaling (26–28), but its role in GBM is less established (29,30) although recent studies suggest its importance in tumor progression (31).

Given the role for HSPGs in tumorigenesis and the importance of GAG composition and structure in regulating cell signaling and invasion, we investigated HS GAGs in GBM using tumorspheres cultured from four patient-derived GBM lines and two murine GBM. In addition, we examine the biologic function of HS modification in tumor cell invasion. These data demonstrate heterogeneity in HS content and structure in GBM and suggest intertumoral differences in proteoglycan expression and function with potential implications for therapeutic stratification.

MATERIALS AND METHODS

Cell culture conditions and reagents

Murine GBM tumorspheres established and demonstrated to have tumor-generating and differentiation capacity in Lindberg O. et al. (32) were cultured and maintained as described previously (21,32,33). GBM43, GBM6, and GBM5 are tumorsphere cultures of patient-derived xenografts (PDX). PDX were established as previously described (34,35) and have been genetically and transcriptionally profiled (1,35,36). GBM1 (SF9487) is a newly generated primary patient-derived tumorsphere culture from UCSF and when injected into the striatum of nude mice generates highly invasive GBM (Supplemental Figure 1, Supplemental Table 1, and Supplemental Material and Methods). All cell lines were analyzed before using and each subsequent year by short tandem repeat (STR) analysis to ensure the identity and validity of cells and checked by PCR for mycoplasma contamination. Cells were passaged no more than 15–20 times and then a new frozen aliquot of cells was used. Unless otherwise specified media and supplements were purchased from Thermo Fisher Scientific (Waltham, MA). Human tumorspheres (2–4 × 10^4 cells/1ml) were cultured in Neurobasal-A media containing B27-A, N2 and glutamine and passaged every 4–7 days. bFGF and EGF were added every third day (20 ng/ml). Tumorspheres were dissociated by adding 2 ml of Accutase (Innovative Cell Technologies, San Diego, CA) (hGBM) or 150 μL non-enzymatic dissociation media (NEDM; Sigma-Aldrich Corporation, St. Louis, MO) (mGBM) followed by mechanical trituration. Invasion assays use Corning® Matrigel® Growth Factor Reduced (GFR) Basement Membrane Matrix (Corning Inc., Corning, NY).

Purification of GAG chains, quantification and disaccharide compositional profiling of HS chains from tumorspheres

GAG chains were purified and analyzed from tumorsphere cultures following the protocol reported by Yang B. et al (2011) (37) with minor modifications (see Supplemental Materials and Methods). The HS disaccharides were released from the GAG chains with heparitinase I, II, III (a kind gift from Dr. Kuberan Balagurunathan) in heparitinase buffer (3.3 mM calcium acetate, 40 mM amonium acetate, 0.1mg/ml BSA, pH 7.0) overnight followed by enzyme inactivation at 100°C for 5 min. Proteins and uncleaved GAG chains were removed using 3 kDa MWCO Amicon columns (12000xg). Heparan sulfate disaccharide were separated by a 5 um particle size Zorbax SB-C18 HPLC column with a 12 mM TrBA/38 mM ammonium acetate, pH 6.5 solvent systems using a gradient curve from 2% to 100%

solvent B (65% acetontrile) at flowrate 10 μl/min with extra acetrontrile (0.7ml/min). The MS was acquired in the negative ion mode with inline 4000 QTRAP mass spectrometry equipped with a TIS (Turbolon Ionspray) source (AB Sciex Instrument. SCIEX, Redwood City, CA) at the following conditions: curtain gas (CUR) at 10 psi, ion spray voltage (IS) at 4500 V, temperature (TEM) at 100°C, ion source gas (GS1) at 10 psi, ion source gas (GS2) at 0 psi, declustering potential (DP) at −50 V, and entrance Potential (EP) was set at −10 V. Quantification analysis of heparin/HS disaccharides was performed using calibration curves constructed from unsaturated heparan sulfate disaccharide (18.6, 37.2, 74.4, 148.8, 297.6, 595.2 ng per disaccharide) (Supplemental Figures 2–3) as described in Supplemental Material and Methods. The area of disaccharides and internal standards was quantified using PeakView 2.2 software (AB Sciex LLC, CA). Total HS amount was calculated as the cumulative total of each disaccharide and to compare across tumors the value was normalized by total protein (ng/mg).

RNA and protein analysis

Tumorspheres were re-suspended in an appropriate volume of RLT buffer from RNeasy mini kit (Qiagen, Germany). RNA was isolated as per the manufacturers instructions and quantified using a Nanodrop (Nanodrop Technologies Inc., Wilmington, DE) Spectrophotometer. For quantitative real time PCR, complementary DNA was synthesized using Oligo(dT) primers and Superscript III (18080-051, Thermo Fisher Scientific). Primers were synthesized by IDT (IDT Inc, Coralville, IA) and are listed in Supplemental Table 2. Real Time PCR was performed on a 7900 HT Fast Real-Time PCR System (Thermo Fisher Scientific, Waltham, MA) using FastStart Universal SYBR Green Master (Rox) (Roche, Switzerland). Ct values were normalized to GAPDH Ct values for each individual sample and then averaged across experiments. For NanoString analysis of human tumorsphere lines, RNA (200ng) integrity was assessed using an Agilent 2100 bioanalyzer (Agilent Technologies, Santa Clara, CA) and probed using a custom codeset, including four genes of interest in GBM (EGFR, EGFRvIII, PDGFRA, and NF1), and 6 normalizing genes (*ACTB*, *B2M*, *GAPDH*, *POLR2A*, *SDHA*, and *TBP*). Data was analyzed with the NanoString nCounter Analysis System at NanoString Technologies according to the manufacturer's protocol (NanoString Technologies, Seattle, WA) and relative expression levels were compared (Supplementary Table 2). Gene expression data from human GBM were downloaded from http://www.cbioportal.org/index.do. Gene expression analysis of mRNA isolated from FACs sorted murine tumors was previously reported (32) and is available in the GEO database (accession number GSE87332). To assess enrichment of GBM subtype genes in murine tumors Gene Set Enrichment Analysis (GSEA) was implemented using the Broad Institute GSEA v2.07 software (http://www.broadinstitute.org/gsea) and subtype signature genes (2). For all GSEA analyses 1000 gene set permutations were performed and a Signal2Noise ranking metric was used to create the ranked list of genes. A false discovery rate (FDR) q-value of less than 0.05 (5%) was considered statistically significant. HPSE protein was detected by Western blotting using anti-HPSE antibody (#APP60766, Aviva System Biology, San Diego, CA). Anti-Hpse antibody binding to both the 50 kDa and 61 kDa bands could be blocked with an HPSE blocking peptide (Supplemental Figure 4A).

CRISPR/Cas9 gene editing of HPSE

Human HPSE targeting CRISPR guide RNA 6 (CCTTCTTGGGATCGAAAATT) in the pLenti-Guide-puro backbone and lentiCas9-Blast (GenScript, Piscataway, NJ) were used to make lentivirus using standard procedures (21). Target sites and specificity were validated using the UCSC Genome Browser. Transduced GBM43 cells were clonally plated, sequenced, and comparisons were made between GBM43-Cas9 and GBM43-gRNA6. Sequencing the targeted HPSE loci confirmed introduction by the Cas9 nuclease of small, mostly frameshift indels/WT, including gRNA6-1 (NM_001098540, c.395-414del) and gRNA6-2 (NM_001098540, c.389-415del). The human HPSE cDNA construct, pIRES2-EGFP/HPSE1 (38) was a kind gift of Dr. Ralph Sanderson (University of Alabama at Birmingham, Birmingham, AL).

Invasion and adhesion assays

Three-dimensional invasion assays were performed as described previously (39) (see Supplemental Material and Methods). Briefly, 500–1000 cells per well were plated in a 96 well round bottom ultra-low attachment plate (Corning Life Sciences, Tewksbury, MA) in standard culture media (100 μl/well) for 3 days. For drug treatment, the cells were treated with heparin (24 h), necuparanib (formerly M402) (a kind gift from Momenta Pharmaceuticals, Cambridge, MA) (6 h), or an equivalent volume of PBS prior to matrigel invasion assay using growth factor reduced matrigel. Images were acquired at 0, 16, 24, and 40 hours after plating. Relative invasion was determined from representative images of each sphere using ImageJ (http://imagej.nih.gov/ij/) by subtracting the solid sphere area from the maximal invaded sphere area and normalizing by the initial sphere area at 0h (Supplemental Figure 5). Adhesion assays were performed in 96 well plates pre-coated with laminin (2 $\mu g/cm^2$) and blocked with 1% BSA in PBS-D for 1–2 h at 37°C. Cells were treated with necuparanib (Necu) or PBS (control) for 24 h, dissociated to single cells, counted ×3, diluted to 2.5×10^4 cells per 100 μL of full growth media, and transferred to the laminin coated wells. Cells were allowed to adhere for 2 hours at 37°C, after which media and non-adherent cells were gently removed, wells were gently washed with ice-cold PBS, and adherent cells were fixed with 4% paraformaldehyde (PFA), incubated on ice for 10 min, and stained with crystal violet as previously described (32,39). Transwell invasion assays were performed using BD BioCoat Growth Factor Reduced Matrigel Invasion chambers (BD Biosciences, San Jose, CA) as described previously (39) (see Supplemental Materials and Methods). HPSE or Control conditioned media was generated from 293T cells incubated in minimal essential media as described in Supplemental Materials and Methods. Images for 3-D invasion, adhesion, and transwell invasion were acquired using a DMI IL LED Leica microscope (Leica, Germany).

Statistics

All statistics were performed using Graph Pad Prism 6.0 software (Graph Pad Software, San Diego, CA). All data are presented as mean ± standard error (SEM). One-way ANOVA, the student's t-test analysis, and Mann-Whitney test were performed at confidence interval levels of 95%.

RESULTS

Human GBM are heterogeneous and can be divided into subtypes based upon transcriptional profiling (1,2). Our previous studies in GBM (21) and our analysis of transcriptional data from The Cancer Genome Atlas (18) suggested differences in HS proteoglycan expression and function across tumor transcriptional subtypes. Heparan sulfate disaccharides consist of repeating units of a glucosamine (N-acetylglucosamine (NAc) or N-sulfate glucosamine (NS)) and uronic acid (glucuronic acid or iduronic acid) that undergo extensive post-translational modifications including sulfation. These modifications greatly alter their functional properties (8). To determine the diversity of heparan sulfate (HS) content and structure in human GBM, we profiled HS disaccharides isolated from patient-derived GBM lines maintained as tumorspheres using liquid chromatography mass spectrometry (LCMS). Tumor cells were cultured as tumorspheres, using neural stem cell conditions including non-adherent growth and minimal essential media, to promote retention of tumor generating cells (40,41). The four human lines were selected based on their diversity of molecular and transcriptional properties, including EGFR amplification and EGFRvIII expression in GBM6, PDGFRA amplification in GBM5, and CDKN2C/p18(INK4c) homozygous deletion in GBM43 (35,36,42). Nanostring analysis of tumorsphere mRNA confirmed differences between the lines, including EGFR and EGFRvIII expression in GBM6, low expression of NF1 in GBM43, and robust expression of PDGFRA in all four lines (Supplemental Table 3). Individual disaccharides were identified and quantified based on standard curves generated from known quantities of individual disaccharides (Supplemental Figures 2–3). Each of the four independent human GBM lines had a unique HS disaccharide ion chromatography profile (Figure 1A–D) and different total HS abundance (ng disaccharide/mg protein) (Figure 1E). GBM5 had two-fold greater absolute abundance of HS disaccharides compared to the other three GBM lines ($p<0.005$). HS structure also differed between GBM as demonstrated by differences in relative disaccharide abundance (Figure 1F). While many disaccharide structures are regulated during biosynthesis, trisulfate disaccharides can be reduced post-synthetically in the extracellular environment by the extracellular endosulfatases, or SULFs, which remove 6-*O* sulfate from trisulfate disaccharides (12,43). GBM5 had the lowest trisulfate abundance relative to the other GBM (Figure 1F (inset), $p<0.05$). GBM5 also had the highest expression of *SULF2* mRNA across the four lines (Figure 1G, **$p<0.0001$**). In contrast, *SULF1* was expressed at similar levels (Figure 1H).

Heparanase (*HPSE*), an HS degrading enzyme, can directly alter cellular HS content (44) and indirectly change cell surface proteoglycan core protein composition via HS-dependent regulation of proteases (45). In several cancers including GBM, HPSE expression is upregulated and has been associated with increased tumor cell invasion and increased tumor growth in vivo (22,46). In human GBM, *HPSE* was most highly expressed in the mesenchymal GBM subtype (Figure 2A; $p<0.0001$), a subtype proposed to be the most therapy resistant (47). To examine potential functions for HPSE in GBM43, CRISPR-Cas9 gene editing was used to introduce deletions in exon 3 of HPSE. Clones with heterozygous deletions in *HPSE* and reduced HPSE expression relative to control clones were isolated (Figure 2B $p<0.001$). HPSE reduced clones did not exhibit a growth defect relative to control clones in vitro (Supplemental Figure 4B). To assess cell invasion in the context of a

three-dimensional matrix, tumorspheres were embedded in matrigel and tumor cell invasion away from the sphere was imaged and quantified over time. Reduced HPSE conferred a marked decrease in tumor cell invasion (Figure 2C–D, $p<0.0001$). Cell invasion in a three-dimensional matrix requires coordinated regulation of cell attachment, migration, and ECM breakdown. Given the reported roles for HPSE and HS in cell invasion and adhesion, we asked whether decreased invasion in HPSE-reduced cells was associated with reduced cell adhesion. *HPSE* reduced GBM43 had markedly reduced cell adhesion to laminin relative to control cells (Figure 2E–F, $p<0.01$). Addition of exogenous HPSE promoted invasion of HPSE-reduced GBM43 cells relative to control treated cells (Figure 2G–H, $p<0.05$).

Heparin, a highly sulfated HS, can bind to and inhibit HS-interacting factors including enzymes such as HPSE (48,49). Due to the anticoagulant properties of heparin, however, heparan sulfate mimetics have been developed with reduced anti-coagulant properties. These mimetics have been used for their ability to inhibit HPSE and the function of other HS-interacting factors in therapeutic trials for cancer, including necuparanib (formerly M402), PI-88, PG-545, and SST0001 (https://clinicaltrials.gov) (Supplemental Table 4). Treating GBM43 with necuparanib (necu), a heparan sulfate mimetic re-engineered from heparin (49), reduced three-dimensional tumor cell invasion (Figure 3A–B, $p<0.001$) and reduced cell adhesion to 53% of control treated cells (Figure 3C, $p<0.01$). Thus, a heparan sulfate mimetic could phenocopy HPSE knockdown supporting a role for HPSE in GBM tumor cell invasion and cell adhesion to laminin.

Human GBM can be subtyped based on transcriptional signatures (1,2), however, multiple sampling of tumors and single-cell analysis suggest tumors retain significant intratumoral heterogeneity even within a given subtype (50). To investigate associations between HS GAG content, structure and role in invasion in a more homogeneous system we used a murine model for GBM driven by defined alterations in neural progenitor cells (21,32) (Figure 4A). First, tumor prone cells, containing alterations common to human GBM (deletion of Ink4a/Arf and expression of EGFRvIII), were implanted orthotopically in mice, and allowed to form invasive tumors. Second, tumor cells were isolated and cultured from tumors as tumorspheres under non-adherent conditions in minimal essential media. Murine tumorspheres maintained in this manner retain tumor-forming capacity and biologic features of the original tumor (32). Previously we identified and transcriptionally profiled tumors from two murine tumorsphere lines with different biologic behaviors (32). Gene Set Enrichment Analysis (GSEA) of differentially expressed genes (GSE87332) demonstrated significant enrichment for mesenchymal signature genes in tumors designated murine mesenchymal-like (mMES) and proneural signature genes in tumors designated murine proneural-like (mPN) (Figure 4B, NES 1.59, FDR q-value <0.001%, and Figure 4C, NES 2.66, FDR q-value <0.0001%, respectively). Using these two tumorsphere lines generated from syngeneic neural progenitor cells, we investigated differences in HS content and HS structure.

HS disaccharides isolated from murine tumorspheres were analyzed by LCMS. Similar to the human tumor cells, each murine line had a unique HS disaccharide ion chromatography profile (Figure 5A–B). mPN had increased total HS abundance (ng disaccharide/mg protein) relative to mMES (Figure 5C, $p<0.05$). While overall HS structure of mMES and mPN was

more similar than when comparing the human GBM, mPN had decreased levels of trisulfate disaccharides relative to mMES (Figure 5D, $p<0.01$). Similar to GBM5 with reduced levels of trisulfate disaccharides, the mPN cells had increased expression of the extracellular endosulfatase Sulf2 for which HS trisulfate disaccharides are a substrate (Figure 5E, $p<0.001$). SULF2 protein expression was also elevated in mPN tumors *in vivo* (Figure 5F) suggesting SULF2 may be one determinant of HS trisulfate abundance in GBM.

To investigate the factors that may influence the reduced HS content in mMES tumor cells we compared expression of HPSE and HS biosynthetic enzymes and core proteins. Hpse expression was markedly different in the two lines with increased *Hpse* mRNA (Figure 6A, $p<0.001$) and protein expression (Figure 6B–C, $p<0.05$) in mMES relative to mPN tumorspheres, including the 52 kDa active enzyme. Biosynthetic enzymes important in HS chain initiation (*Xylt1*) and elongation (*Ext1*) were also decreased in mMES relative to mPN (Figure 6D, $p<0.0001$). In addition, expression of the core protein Syndecan 3 (Sdc3) was significantly decreased in mMES cells ($p<0.05$) (Figure 6E). These data suggest several factors may contribute to the lower abundance of total HS in mMES versus mPN, including decreased expression of HS biosynthetic enzymes, decreased expression of core proteins such as *Sdc3*, and increased expression of the HS degrading enzyme *Hpse*.

Based on our data with human tumorspheres, we treated murine tumorspheres with either heparin or the heparan sulfate mimetic necuparanib to investigate HS function in tumor cell invasion. Treatment of *Hpse*-high mMES cells with heparin inhibited invasion in three-dimensional matrigel invasion assays in a dose-dependent manner (Figure 7A–B, $p<0.05$). In contrast, invasion of *Hpse*-low mPN cells was not decreased by heparin (Figure 7C). Similar to treatment with heparin, HS mimetic treatment inhibited invasion of *Hpse*-high mMES cells (Figure 7D–E, $p<0.05$).

DISCUSSION

GBM are highly malignant, invasive tumors that are highly resistant to current therapies and associated with a dismal prognosis. HS proteoglycans on the cell surface and in the extracellular matrix regulate interactions in the extracellular environment such as ligand-mediated signaling, a potential mechanism of resistance to targeted therapies (51). Analysis of tumorspheres derived from four patient-derived GBM (hGBM) lines and two murine GBM lines demonstrate heterogeneity in the content and the structure of HS glycosaminoglycans. Patient-derived GBM5 and mPN demonstrated increased HS content, increased SULF2 expression and reduced HS trisulfate groups, the major substrate for SULF2. These data support previous studies in human GBM demonstrating that SULF2, an extracellular endosulfatase that removes 6-*O*-sulfate from trisulfate disaccharides and can promote PDGFRA signaling, is most highly expressed in a subset of GBM (21). In contrast, GBM43 and mMES tumorspheres exhibited elevated expression of the HS-modifying enzyme HPSE. Heterozygous gene deletion of HPSE in human GBM tumorspheres decreased tumor cell invasion and adhesion. Chemical inhibition of HS function reduced human and murine tumorsphere invasion and this was most pronounced in HPSE-high cells. These data support a role for HS-interacting factors, including HPSE, in tumor invasion and highlight the heterogeneity of HS content, structure, and function in GBM.

HPSE specifically liberates biologically active GAG chains from HSPGs, and its activity is associated with both cell autonomous and non-cell autonomous functions (reviewed in (22)). HPSE can promote tumor cell invasion in several ways, including actions on HSPGs on the cell surface and in the extracellular matrix (10,26,27,52,53). In multiple myeloma HPSE promotes tumor cell adhesion and invasion via SDC1 ectodomain shedding and subsequent alterations in receptor tyrosine kinase signaling and integrin binding (10,23,54). Few studies have investigated the role for HPSE in primary brain tumors (28–31,46), but the data suggest HPSE can promote tumor growth and progression in vivo. HPSE knockdown in human GBM43 cells cultured under neural stem cell conditions did not alter proliferation. The role for HPSE in proliferation in vitro may be complex and potential modifiers include cell culture conditions, cell lines used, and method to alter HPSE levels (31,46). In human GBM, HPSE is most highly expressed in the mesenchymal GBM subtype. In tumorsphere lines derived from both human and murine GBM, we identify elevated HPSE expression in a subset of tumors, and HPSE knockdown in human GBM43 or inhibition of HS function in human GBM43 or mMES tumorspheres reduced tumor cell invasion. While the regulators of HPSE expression in GBM are not known, the NF-κB pathway, active in a subset of GBM with a radioresistant and mesenchymal phenotype (47), can drive HPSE expression following viral infection (44).

HSPGs regulate signaling pathways important in cell proliferation, inflammation, angiogenesis, and invasion and are dysregulated in cancer (reviewed in (18) and (55)). As extracellular molecules, HSPGs and the extracellular enzymes that modify them, SULF2 and HPSE, are amenable to therapeutic targeting. HS mimetics, highly sulfated oligosaccharides, inhibit HS-binding enzymes such as the SULFs and HPSE, as well as sequester HS-binding ligands, making them attractive candidates for cancer therapy (56,57). In preclinical studies, HS mimetics have effectively targeted multiple HSPG-dependent phenotypes, as indicated by their ability to decrease tumor growth, invasion, metastasis and angiogenesis (49,58). While HS mimetics have not yet been tested in GBM in vivo, our data suggest that HS mimetics or more selective inhibitors of proteoglycan function may have anti-tumor efficacy in subsets of GBM patients.

Using human and murine GBMs, our study identifies different patterns of proteoglycan expression and modification in tumors and demonstrates a role for HPSE in tumor invasion. Recent advances in glycan analysis from cells and tissue (59–62) open the way for a detailed analysis of glycan structure and content in human tumors. The integration of detailed glycomic, genomic, and proteomic data will facilitate the identification of novel tumor biomarkers and help to identify tumors most likely to respond to inhibitors of HSPG function.

Supplementary Material

Refer to Web version on PubMed Central for supplementary material.

Acknowledgments

Financial support: This study was funded by NIH/NINDS R01 NS081117 to J.J.P., NIH/NCI U01 CA168878 to J.J.P., and resources were provided by NIH Grant PO1-HL107152 to B.K. Mass spectrometry was performed at the

UCSF Mass Spec Facility (NIH NCRR P41RR001614). The content is solely the responsibility of the authors and does not necessarily represent the official views of the National Institutes of Health.

We thank Drs. Kuberan Balagurunathan, Steven D. Rosen, and Ralph Sanderson for sharing their expertise and reagents. We also thank Dr. Kuberan Balagurunathan for providing us with heparitinase I,II,III. Necuparanib (formerly M402) was generously provided by Momenta Pharmaceuticals (Cambridge, MA) with special thanks to Amanda MacDonald, Birgit Schultes, and Silva Krause. We also acknowledge the UCSF Brain Tumor SPORE Tissue Core (P50CA097257) for providing de-identified GBM tissue for establishment of GBM1 tumorspheres.

References

1. Verhaak RGW, Hoadley KA, Purdom E, Wang V, Qi Y, Wilkerson MD, et al. Integrated Genomic Analysis Identifies Clinically Relevant Subtypes of Glioblastoma Characterized by Abnormalities in PDGFRA, IDH1, EGFR, and NF1. Cancer Cell. 2010; 17:98–110. [PubMed: 20129251]
2. Phillips HS, Kharbanda S, Chen R, Forrest WF, Soriano RH, Wu TD, et al. Molecular subclasses of high-grade glioma predict prognosis, delineate a pattern of disease progression, and resemble stages in neurogenesis. Cancer Cell. 2006; 9:157–73. [PubMed: 16530701]
3. Stommel JM, Kimmelman AC, Ying H, Nabioullin R, Ponugoti AH, Wiedemeyer R, et al. Coactivation of receptor tyrosine kinases affects the response of tumor cells to targeted therapies. Science. 2007; 318:287–90. [PubMed: 17872411]
4. Brennan C, Momota H, Hambardzumyan D, Ozawa T, Tandon A, Pedraza A, et al. Glioblastoma Subclasses Can Be Defined by Activity among Signal Transduction Pathways and Associated Genomic Alterations. PLOS ONE. 2009; 4:e7752. [PubMed: 19915670]
5. Wood MD, Reis GF, Reuss DE, Phillips JJ. Protein Analysis of Glioblastoma Primary and Posttreatment Pairs Suggests a Mesenchymal Shift at Recurrence. J Neuropathol Exp Neurol. 2016:nlw068.
6. Engler JR, Robinson AE, Smirnov I, Hodgson JG, Berger MS, Gupta N, et al. Increased Microglia/Macrophage Gene Expression in a Subset of Adult and Pediatric Astrocytomas. PLOS ONE. 2012; 7:e43339. [PubMed: 22937035]
7. WangQ, , HuX, , HuB, , MullerF, , KimH, , SquatritoM. , et al. Tumor evolution of glioma intrinsic gene expression subtype associates with immunological changes in the microenvironment [Internet]2016May. Report No.: biorxiv;052076v3. Available from: http://biorxiv.org/lookup/doi/10.1101/052076
8. Bishop JR, Schuksz M, Esko JD. Heparan sulphate proteoglycans fine-tune mammalian physiology. Nature. 2007; 446:1030–7. [PubMed: 17460664]
9. Rapraeger AC, Krufka A, Olwin BB. Requirement of heparan sulfate for bFGF-mediated fibroblast growth and myoblast differentiation. Science. 1991; 252:1705–8. [PubMed: 1646484]
10. Jung O, Trapp-Stamborski V, Purushothaman A, Jin H, Wang H, Sanderson RD, et al. Heparanase-induced shedding of syndecan-1/CD138 in myeloma and endothelial cells activates VEGFR2 and an invasive phenotype: prevention by novel synstatins. Oncogenesis. 2016; 5:e202. [PubMed: 26926788]
11. Bülow HE, Hobert O. Differential Sulfations and Epimerization Define Heparan Sulfate Specificity in Nervous System Development. Neuron. 2004; 41:723–36. [PubMed: 15003172]
12. Ai X, Do A-T, Kusche-Gullberg M, Lindahl U, Lu K, Emerson CP. Substrate Specificity and Domain Functions of Extracellular Heparan Sulfate 6-O-Endosulfatases, QSulf1 and QSulf2. J Biol Chem. 2006; 281:4969–76. [PubMed: 16377625]
13. Ai X, Do A-T, Lozynska O, Kusche-Gullberg M, Lindahl U, Emerson CP. QSulf1 remodels the 6-O sulfation states of cell surface heparan sulfate proteoglycans to promote Wnt signaling. J Cell Biol. 2003; 162:341–51. [PubMed: 12860968]
14. Ai X, Kitazawa T, Do A-T, Kusche-Gullberg M, Labosky PA, Emerson CP. SULF1 and SULF2 regulate heparan sulfate-mediated GDNF signaling for esophageal innervation. Dev Camb Engl. 2007; 134:3327–38.
15. Danesin C, Agius E, Escalas N, Ai X, Emerson C, Cochard P, et al. Ventral Neural Progenitors Switch toward an Oligodendroglial Fate in Response to Increased Sonic Hedgehog (Shh) Activity: Involvement of Sulfatase 1 in Modulating Shh Signaling in the Ventral Spinal Cord. J Neurosci. 2006; 26:5037–48. [PubMed: 16687495]

16. Dhoot GK, Gustafsson MK, Ai X, Sun W, Standiford DM, Emerson CP. Regulation of Wnt Signaling and Embryo Patterning by an Extracellular Sulfatase. Science. 2001; 293:1663–6. [PubMed: 11533491]

17. Uchimura K, Morimoto-Tomita M, Bistrup A, Li J, Lyon M, Gallagher J, et al. HSulf-2, an extracellular endoglucosamine-6-sulfatase, selectively mobilizes heparin-bound growth factors and chemokines: effects on VEGF, FGF-1, and SDF-1. BMC Biochem. 2006; 7:2. [PubMed: 16417632]

18. Wade A, Robinson AE, Engler JR, Petritsch C, James CD, Phillips JJ. Proteoglycans and their roles in brain cancer. FEBS J. 2013; 280:2399–417. [PubMed: 23281850]

19. Johansson FK, Brodd J, Eklöf C, Ferletta M, Hesselager G, Tiger C-F, et al. Identification of candidate cancer-causing genes in mouse brain tumors by retroviral tagging. Proc Natl Acad Sci U S A. 2004; 101:11334–7. [PubMed: 15273287]

20. Johansson FK, Göransson H, Westermark B. Expression analysis of genes involved in brain tumor progression driven by retroviral insertional mutagenesis in mice. Oncogene. 2005; 24:3896–905. [PubMed: 15750623]

21. Phillips JJ, Huillard E, Robinson AE, Ward A, Lum DH, Polley M-Y, et al. Heparan sulfate sulfatase SULF2 regulates PDGFRα signaling and growth in human and mouse malignant glioma. J Clin Invest. 2012; 122:911–22. [PubMed: 22293178]

22. Vlodavsky I, Beckhove P, Lerner I, Pisano C, Meirovitz A, Ilan N, et al. Significance of Heparanase in Cancer and Inflammation. Cancer Microenviron. 2011; 5:115–32. [PubMed: 21811836]

23. Purushothaman A, Babitz SK, Sanderson RD. Heparanase Enhances the Insulin Receptor Signaling Pathway to Activate Extracellular Signal-regulated Kinase in Multiple Myeloma. J Biol Chem. 2012; 287:41288–96. [PubMed: 23048032]

24. Purushothaman A, Uyama T, Kobayashi F, Yamada S, Sugahara K, Rapraeger AC, et al. Heparanase-enhanced shedding of syndecan-1 by myeloma cells promotes endothelial invasion and angiogenesis. Blood. 2010; 115:2449–57. [PubMed: 20097882]

25. Ramani VC, Yang Y, Ren Y, Nan L, Sanderson RD. Heparanase Plays a Dual Role in Driving Hepatocyte Growth Factor (HGF) Signaling by Enhancing HGF Expression and Activity. J Biol Chem. 2011; 286:6490–9. [PubMed: 21131364]

26. Marchetti D. Specific degradation of subendothelial matrix proteoglycans by brain-metastatic melanoma and brain endothelial cell heparanases. J Cell Physiol. 1997; 172:334–42. [PubMed: 9284953]

27. Marchetti D, Li J, Shen R. Astrocytes Contribute to the Brain-metastatic Specificity of Melanoma Cells by Producing Heparanase. Cancer Res. 2000; 60:4767–70. [PubMed: 10987284]

28. Ridgway LD, Wetzel MD, Marchetti D. Heparanase Modulates Shh and Wnt3a Signaling in Human Medulloblastoma Cells. Exp Ther Med. 2011; 2:229–38. [PubMed: 21442027]

29. Hong X, Nelson KK, deCarvalho AC, Kalkanis SN. Heparanase expression of glioma in human and animal models. J Neurosurg. 2010; 113:261–9. [PubMed: 19835469]

30. Ueno Y, Yamamoto M, Vlodavsky I, Pecker I, Ohshima K, Fukushima T. Decreased expression of heparanase in glioblastoma multiforme. J Neurosurg. 2005; 102:513–21. [PubMed: 15796387]

31. Kundu S, Xiong A, Spyrou A, Wicher G, Marinescu VD, Edqvist P-HD, et al. Heparanase Promotes Glioma Progression and Is Inversely Correlated with Patient Survival. Mol Cancer Res MCR. 2016; 14:1243–53. [PubMed: 27565180]

32. Lindberg OR, McKinney A, Engler JR, Koshkakaryan G, Gong H, Robinson AE, et al. GBM heterogeneity as a function of variable epidermal growth factor receptor variant III activity. Oncotarget. 2016

33. Bachoo RM, Maher EA, Ligon KL, Sharpless NE, Chan SS, You MJ, et al. Epidermal growth factor receptor and Ink4a/Arf: Convergent mechanisms governing terminal differentiation and transformation along the neural stem cell to astrocyte axis. Cancer Cell. 2002; 1:269–77. [PubMed: 12086863]

34. Sarkaria JN, Carlson BL, Schroeder MA, Grogan P, Brown PD, Giannini C, et al. Use of an orthotopic xenograft model for assessing the effect of epidermal growth factor receptor

amplification on glioblastoma radiation response. Clin Cancer Res Off J Am Assoc Cancer Res. 2006; 12:2264–71.

35. Giannini C, Sarkaria JN, Saito A, Uhm JH, Galanis E, Carlson BL, et al. Patient tumor EGFR and PDGFRA gene amplifications retained in an invasive intracranial xenograft model of glioblastoma multiforme. Neuro-Oncol. 2005; 7:164–76. [PubMed: 15831234]
36. Hodgson JG, Yeh R-F, Ray A, Wang NJ, Smirnov I, Yu M, et al. Comparative analyses of gene copy number and mRNA expression in glioblastoma multiforme tumors and xenografts. Neuro-Oncol. 2009; 11:477–87. [PubMed: 19139420]
37. Yang B, Weyers A, Baik JY, Sterner E, Sharfstein S, Mousa SA, et al. Ultra-performance ion-pairing liquid chromatography with on-line electrospray ion trap mass spectrometry for heparin disaccharide analysis. Anal Biochem. 2011; 415:59–66. [PubMed: 21530482]
38. Kelly T, Suva LJ, Huang Y, Macleod V, Miao H-Q, Walker RC, et al. Expression of heparanase by primary breast tumors promotes bone resorption in the absence of detectable bone metastases. Cancer Res. 2005; 65:5778–84. [PubMed: 15994953]
39. Wade A, Engler JR, Tran VM, Phillips JJ. Measuring sulfatase expression and invasion in glioblastoma. Methods Mol Biol Clifton NJ. 2015; 1229:507–16.
40. Xie Y, Bergström T, Jiang Y, Johansson P, Marinescu VD, Lindberg N, et al. The Human Glioblastoma Cell Culture Resource: Validated Cell Models Representing All Molecular Subtypes. EBioMedicine. 2015; 2:1351–63. [PubMed: 26629530]
41. Lee J, Kotliarova S, Kotliarov Y, Li A, Su Q, Donin NM, et al. Tumor stem cells derived from glioblastomas cultured in bFGF and EGF more closely mirror the phenotype and genotype of primary tumors than do serum-cultured cell lines. Cancer Cell. 2006; 9:391–403. [PubMed: 16697959]
42. Cen L, Carlson BL, Schroeder MA, Ostrem JL, Kitange GJ, Mladek AC, et al. p16-Cdk4-Rb axis controls sensitivity to a cyclin-dependent kinase inhibitor PD0332991 in glioblastoma xenograft cells. Neuro-Oncol. 2012; 14:870–81. [PubMed: 22711607]
43. Morimoto-Tomita M, Uchimura K, Werb Z, Hemmerich S, Rosen SD. Cloning and Characterization of Two Extracellular Heparin-degrading Endosulfatases in Mice and Humans. J Biol Chem. 2002; 277:49175–85. [PubMed: 12368295]
44. Hadigal SR, Agelidis AM, Karasneh GA, Antoine TE, Yakoub AM, Ramani VC, et al. Heparanase is a host enzyme required for herpes simplex virus-1 release from cells. Nat Commun. 2015; 6:6985. [PubMed: 25912399]
45. Purushothaman A, Chen L, Yang Y, Sanderson RD. Heparanase Stimulation of Protease Expression Implicates It as a Master Regulator of the Aggressive Tumor Phenotype in Myeloma. J Biol Chem. 2008; 283:32628–36. [PubMed: 18812315]
46. Zetser A, Bashenko Y, Miao H-Q, Vlodavsky I, Ilan N. Heparanase affects adhesive and tumorigenic potential of human glioma cells. Cancer Res. 2003; 63:7733–41. [PubMed: 14633698]
47. Bhat KPL, Balasubramaniyan V, Vaillant B, Ezhilarasan R, Hummelink K, Hollingsworth F, et al. Mesenchymal differentiation mediated by NF-κB promotes radiation resistance in glioblastoma. Cancer Cell. 2013; 24:331–46. [PubMed: 23993863]
48. Bar-Ner M, Eldor A, Wasserman L, Matzner Y, Cohen IR, Fuks Z, et al. Inhibition of heparanase-mediated degradation of extracellular matrix heparan sulfate by non-anticoagulant heparin species. Blood. 1987; 70:551–7. [PubMed: 2955820]
49. Zhou H, Roy S, Cochran E, Zouaoui R, Chu CL, Duffner J, et al. M402, a Novel Heparan Sulfate Mimetic, Targets Multiple Pathways Implicated in Tumor Progression and Metastasis. PLOS ONE. 2011; 6:e21106. [PubMed: 21698156]
50. Patel AP, Tirosh I, Trombetta JJ, Shalek AK, Gillespie SM, Wakimoto H, et al. Single-cell RNA-seq highlights intratumoral heterogeneity in primary glioblastoma. Science. 2014; 344:1396–401. [PubMed: 24925914]
51. Wilson TR, Fridlyand J, Yan Y, Penuel E, Burton L, Chan E, et al. Widespread potential for growth-factor-driven resistance to anticancer kinase inhibitors. Nature. 2012; 487:505–9. [PubMed: 22763448]

52. Roy M, Marchetti D. Cell surface heparan sulfate released by heparanase promotes melanoma cell migration and angiogenesis. J Cell Biochem. 2009; 106:200–9. [PubMed: 19115257]

53. Roy M, Reiland J, Murry BP, Chouljenko V, Kousoulas KG, Marchetti D. Antisense-mediated suppression of Heparanase gene inhibits melanoma cell invasion. Neoplasia N Y N. 2005; 7:253–62.

54. Edovitsky E, Elkin M, Zcharia E, Peretz T, Vlodavsky I. Heparanase Gene Silencing, Tumor Invasiveness, Angiogenesis, and Metastasis. JNCI J Natl Cancer Inst. 2004; 96:1219–30. [PubMed: 15316057]

55. Vicente CM, Lima MA, Yates EA, Nader HB, Toma L. Enhanced tumorigenic potential of colorectal cancer cells by extracellular sulfatases. Mol Cancer Res MCR. 2015; 13:510–23. [PubMed: 25477293]

56. Dredge K, Hammond E, Handley P, Gonda TJ, Smith MT, Vincent C, et al. PG545, a dual heparanase and angiogenesis inhibitor, induces potent anti-tumour and anti-metastatic efficacy in preclinical models. Br J Cancer. 2011; 104:635–42. [PubMed: 21285983]

57. Hossain MM, Hosono-Fukao T, Tang R, Sugaya N, van Kuppevelt TH, Jenniskens GJ, et al. Direct detection of HSulf-1 and HSulf-2 activities on extracellular heparan sulfate and their inhibition by PI-88. Glycobiology. 2010; 20:175–86. [PubMed: 19822709]

58. Joyce JA, Freeman C, Meyer-Morse N, Parish CR, Hanahan D. A functional heparan sulfate mimetic implicates both heparanase and heparan sulfate in tumor angiogenesis and invasion in a mouse model of multistage cancer. Oncogene. 2005; 24:4037–51. [PubMed: 15806157]

59. Li B, Liu H, Zhang Z, Stansfield HE, Dordick JS, Linhardt RJ. Analysis of glycosaminoglycans in stem cell glycomics. Methods Mol Biol Clifton NJ. 2011; 690:285–300.

60. Li G, Li L, Tian F, Zhang L, Xue C, Linhardt RJ. Glycosaminoglycanomics of cultured cells using a rapid and sensitive LC-MS/MS approach. ACS Chem Biol. 2015; 10:1303–10. [PubMed: 25680304]

61. Shao C, Shi X, Phillips JJ, Zaia J. Mass spectral profiling of glycosaminoglycans from histological tissue surfaces. Anal Chem. 2013; 85:10984–91. [PubMed: 24099043]

62. Weyers A, Yang B, Yoon DS, Park J-H, Zhang F, Lee KB, et al. A structural analysis of glycosaminoglycans from lethal and nonlethal breast cancer tissues: toward a novel class of theragnostics for personalized medicine in oncology? Omics J Integr Biol. 2012; 16:79–89.

63. McLendon R, Friedman A, Bigner D, Meir EGV, Brat DJ, Mastrogianakis GM, et al. Comprehensive genomic characterization defines human glioblastoma genes and core pathways. Nature. 2008; 455:1061–8. [PubMed: 18772890]

Implications

Heparan sulfate interacting factors promote GBM invasion and are potential therapeutic targets.

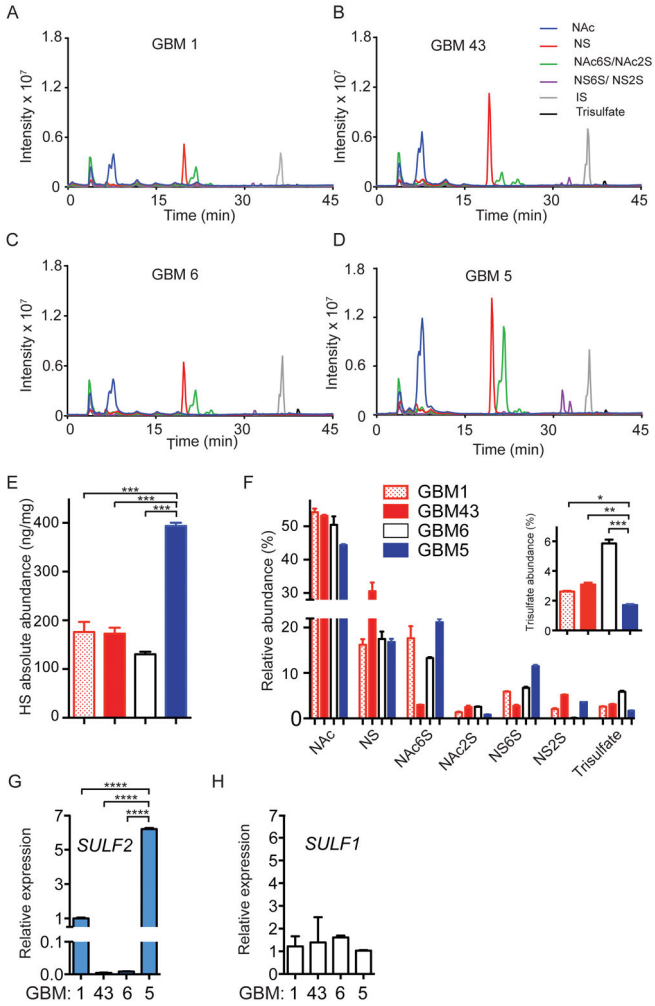

Figure 1. Analysis of HS disaccharide structure and amount from human GBM tumorspheres

(**A–D**) Extracted ion chromatography profile of HS disaccharides isolated from human GBM tumorspheres demonstrating intensity profiles (counts per second) over time (min) across tumors. Based on the analysis of disaccharide standards (Supplemental Figures 2–3), each peak could be assigned a disaccharide with different sulfate patterns. (**E**) Absolute HS abundance normalized to total protein extracted (ng/mg) across tumorspheres. (**F**) Relative HS disaccharide abundance as a percentage (%) of HS disaccharide composition. Inset highlights the comparison of the relative percentage of trisulfate content. (**G–H**) Relative SULF1 and SULF2 gene expression levels in tumorspheres, normalized to GBM43 (n=3). Representative data (A–D) from biologic replicates. Symbols denote: NAc, N-acetylglucosamine; NS, N-sulfated glycosamine; 6S, 6-O-sulfated glucosamine; 2S, 2-O-sulfated iduronic acid; and trisulfate, NS2S6S. Mean ± SEM. *, $p<0.05$; **, $p<0.01$; ***, $p<0.001$; ****, $p<0.0001$.

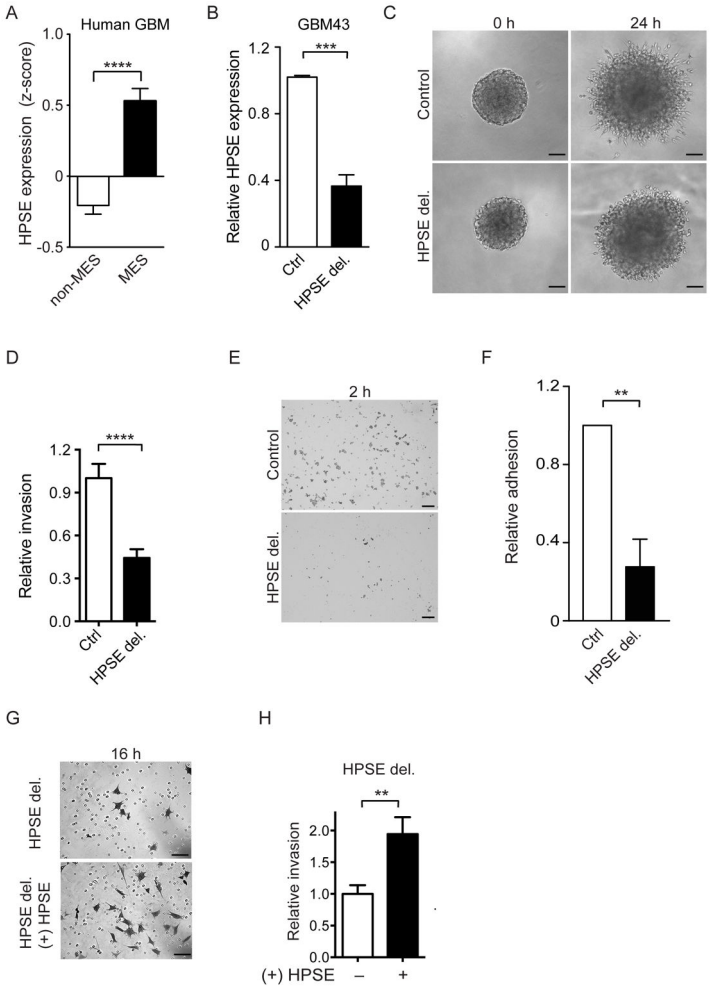

Figure 2. HPSE expression is increased in the mesenchymal GBM subtype and can promote tumor cell invasion

(**A**) Increased expression of HPSE in human GBM of the mesenchymal (MES) transcriptional subtype. Bars denote the mean ± SEM Z-score for tumors in the specified subtype (1) with mesenchymal (red) (n=56) and non-mesenchymal (white) (n=139); The Cancer Genome Atlas (TCGA) Data Portal (63). (**B**) Focal deletion in HPSE confers decreased HPSE mRNA expression in human GBM43 (HPSE del., n=7, and Ctrl, n=3). (**C–D**) Decreased 3D invasion of GBM43 with HPSE deletion as compared to Ctrl. Representative images and quantification (biologic triplicate) at 24 h post plating. (**E–F**) Decreased laminin adhesion of GBM43 with HPSE deletion relative to Ctrl. (**G–H**). Increased invasion of HPSE deletion GBM43 cells treated with conditioned media from HPSE overexpressing cells as compared to control vector (Ctrl) overexpressing cells (HPSE, n=5, and Ctrl, n=5). Mean ± SEM. Representative images and data are from biologic triplicate experiments; *, $p<0.05$; **, $p<0.01$; ***, $p<0.001$; ****, $p<0.0001$. (C, F, H) Scale bars denote 100μm and (E) scale bar denotes 20μm.

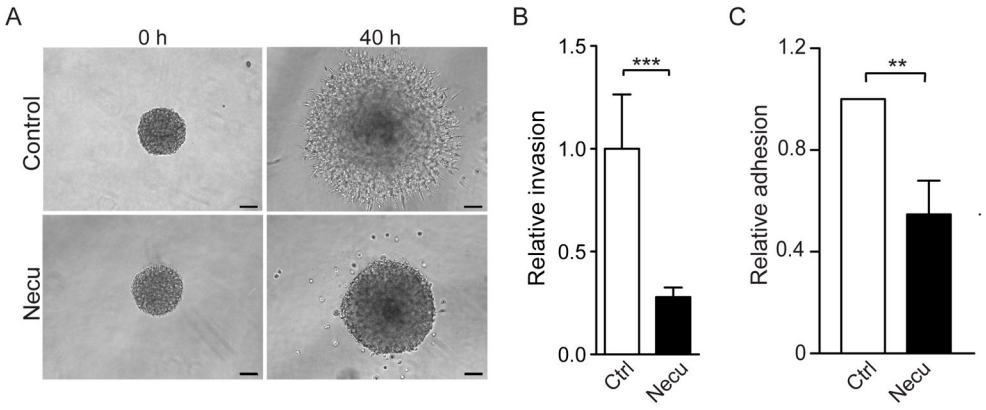

Figure 3. Inhibition of GBM43 invasion and adhesion by a heparan sulfate mimetic

(**A,B**) Decreased 3D invasion of GBM43 following treatment with the heparan sulfate mimetic necuparanib (Necu; 240μg/mL). Representative images and quantification at 40 h post plating (Necu, n=13, Ctrl, n=4). (**C**) Decreased adhesion of Necu treated GBM43 as compared to Ctrl (biologic triplicate). Mean ± SEM. Representative data are from biologic triplicate experiments; **, $p<0.01$; ***, $p<0.001$. Scale bars denote 100μm.

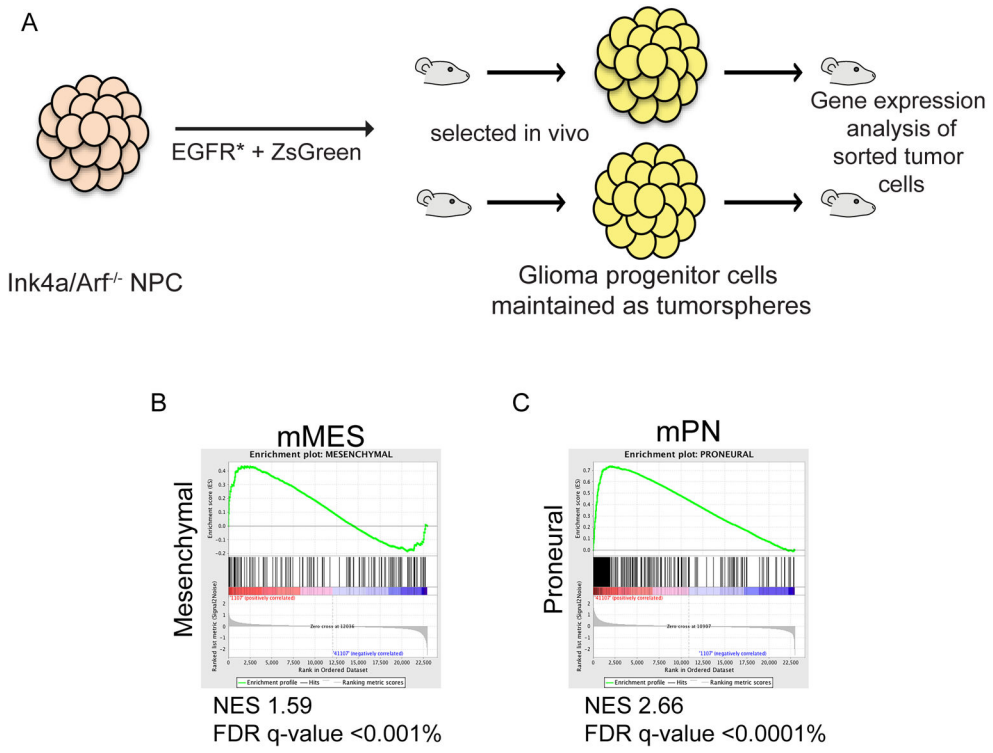

Figure 4. Gene expression analysis of murine tumor cells

(**A**) Murine tumorspheres were derived from brain tumors formed from Ink4a/Arf$^{-/-}$ neural progenitor cells (NPCs) transduced with a constitutively active deletion mutant of EGFR (EGFRvIII; EGFR*) and a fluorescent tag (ZsGreen). Gene set enrichment analysis (GSEA) of differentially expressed genes in tumorsphere-generated tumors (n=6 mice per line, (32)), isolated by fluorescence-activated cell sorting (FACS), revealed differential enrichment of genes associated with human GBM transcriptional subtypes (2). (**B**) Tumors enriched for the human mesenchymal GBM subtype gene signature were denoted murine mesenchymal-like (mMES), NES 1.59, FDR q-value <0.001%. (**C**) Tumors enriched for the human proneural GBM subtype gene signature were denoted murine proneural-like (mPN), NES 2.66, FDR q-value <0.0001%.

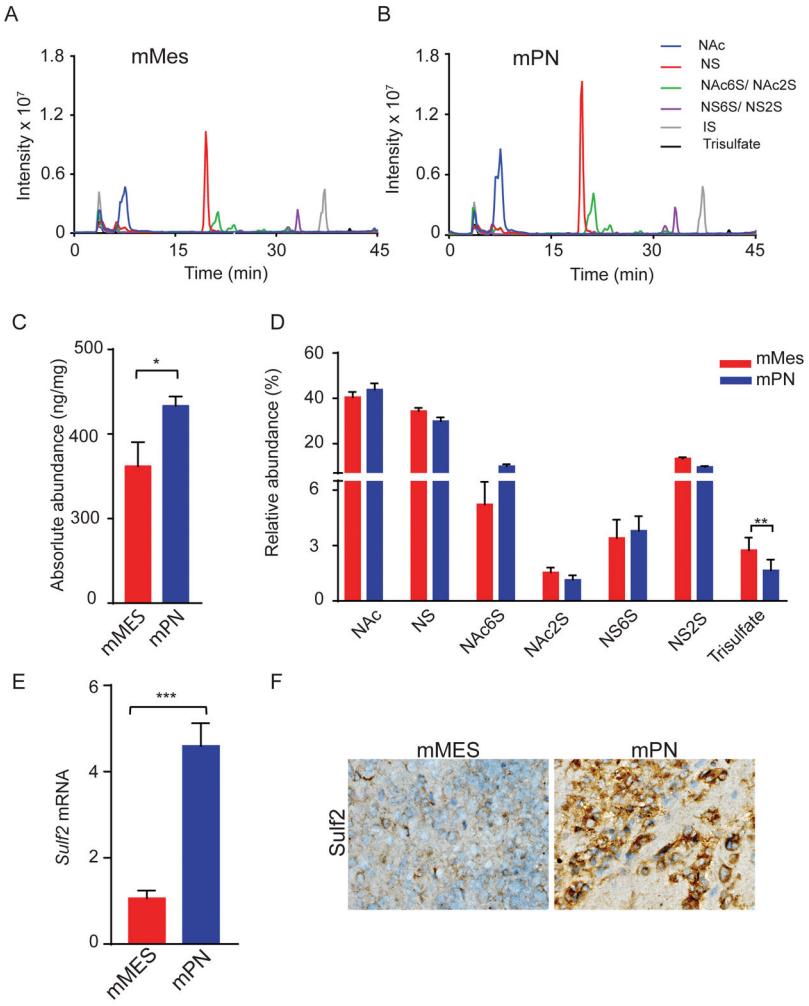

Figure 5. HS disaccharide analysis of mMES and mPN tumorspheres

GAG chains isolated from mMES and mPN tumorspheres were analyzed as in Figure 1. (**A,B**) Extracted ion chromatography profile of HS disaccharides demonstrating differences in HS structure, intensity profiles (counts per second) over time (min). (**C**) Elevated total HS content in mPN as compared to mMES normalized to total protein extracted (ng/mg). (**D**) Relative abundance of HS disaccharide composition in tumorspheres demonstrating decreased trisulfate content in mPN. (**E**) Increased expression of *Sulf2* mRNA in mPN relative to mMES. (**F**) Increased SULF2 protein expression in mPN brain tumors as compared to mMES. (A–B, F) Representative data from 4 biologic replicates. Mean ± SEM. *, $p<0.05$, (n=4); **, $p<0.01$, (n=4); ***, $p<0.001$ (n=5).

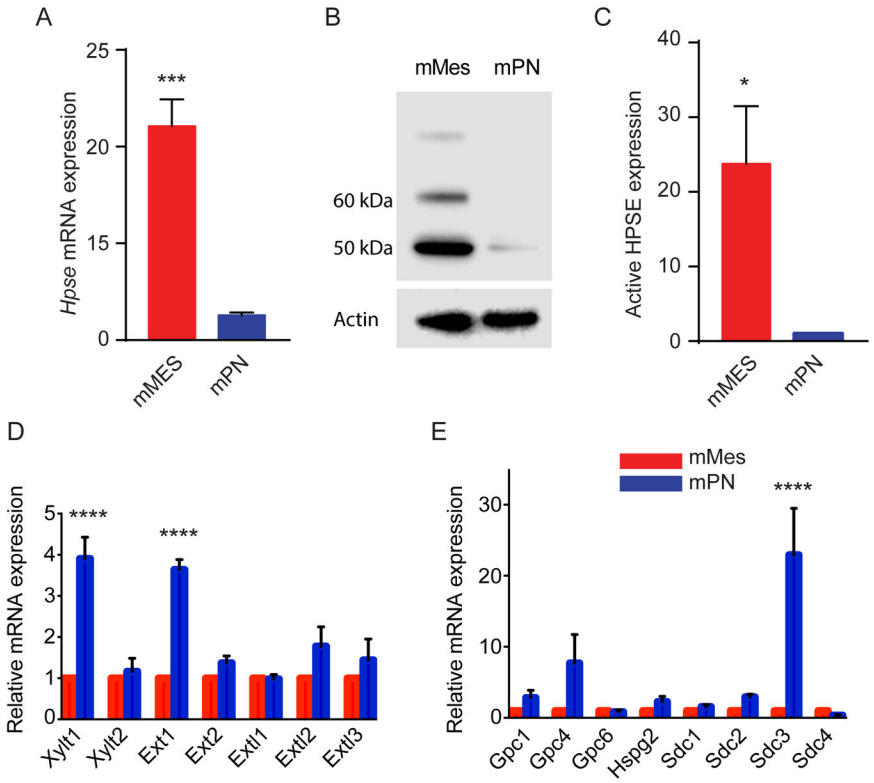

Figure 6. Increased HPSE and decreased HS biosynthetic enzyme and core protein expression in mMes

Tumorspheres from mMES demonstrate increased *Hpse* mRNA (**A**) and protein (**B**) expression as compared to mPN. (**C**) Quantification of 52 kDa active enzyme levels. (**D**) Decreased expression of HS biosynthetic enzymes *Xylt1* and *Ext1* in mMES relative to mPN. (**E**) Decreased *Sdc3* expression in mMES relative to mPN. *, $p<0.05$; **, $p<0.01$; ; ***, $p<0.001$; ****, $p<0.0001$. Mean ± SEM, at least biologic triplicate.

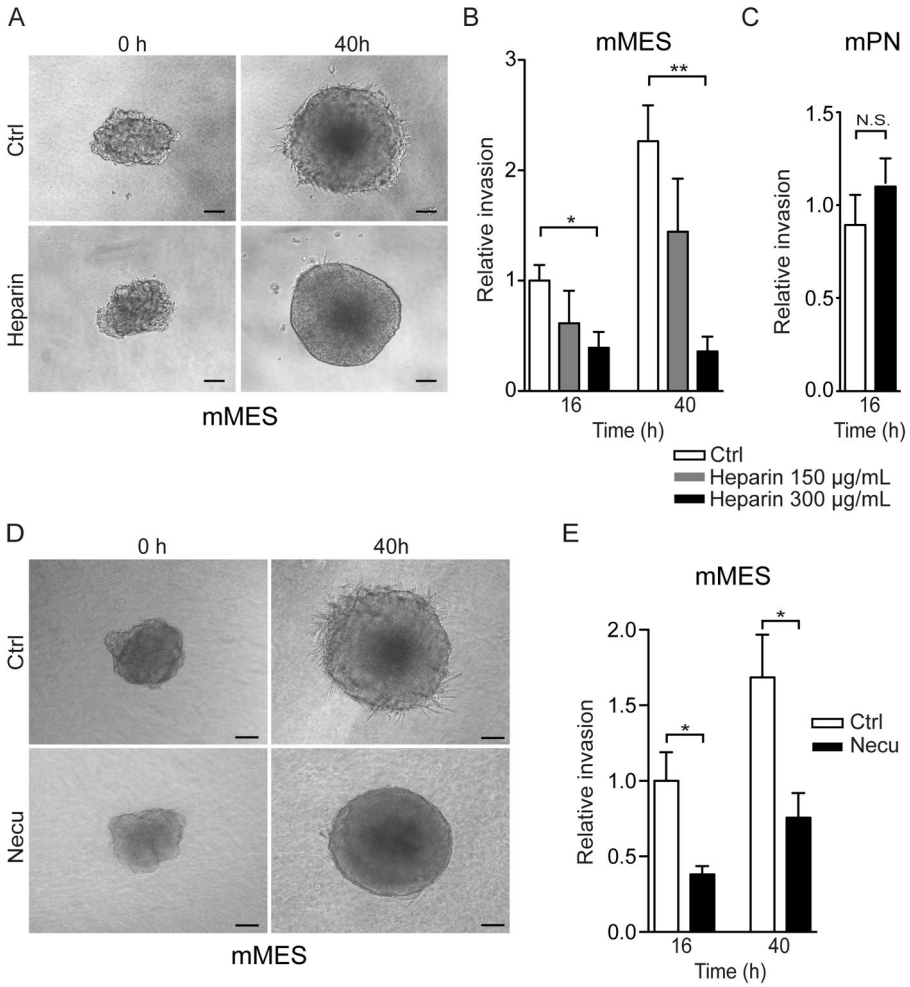

Figure 7. Inhibitors of HS function inhibit invasion in HPSE-high tumorspheres

(**A,B**) Heparin inhibits mMES invasion in a dose-dependent manner in 3D spheroid invasion assays. (**A**) Representative images of Control (Ctrl) and heparin (300 and 150µg/ml) treated mMES tumorspheres at 40 hours (h) and (**B**) quantification at 16h and 40h. (**C**) In contrast, heparin treatment of mPN tumorspheres had no effect on invasion even at the highest concentration (300 µg/ml) at 16 hours. (D–**E**) The heparan sulfate mimetic necuparanib (Necu) also reduced invasion of mMES tumorspheres in 3D invasion assays. Representative images at 40h (**E**) and quantification at 16h and 40h (**F**). Assays performed in biologic triplicate. Mean ± SEM. (B) *, $p<0.05$ and **, $p<0.01$, Ctrl (n= 6), heparin 150 µg/ml (n = 5), and heparin 300 µg/ml (n= 6). *, $p<0.05$, Ctrl and Necu (n=5 each). N.S., not significant (n=6). Scale bars denote 100µm.